NASA/CR-2003-212689

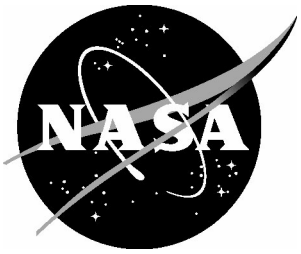

Numerical Analysis of the SCHOLAR Supersonic Combustor

Carlos G. Rodriguez
Allied Aerospace, GASL Division, Hampton, Virginia

Andrew D. Cutler
The George Washington University
Joint Institute for Advancement of Flight Sciences
Langley Research Center, Hampton, Virginia

December 2003

The NASA STI Program Office . . . in Profile

Since its founding, NASA has been dedicated to the advancement of aeronautics and space science. The NASA Scientific and Technical Information (STI) Program Office plays a key part in helping NASA maintain this important role.

The NASA STI Program Office is operated by Langley Research Center, the lead center for NASA's scientific and technical information. The NASA STI Program Office provides access to the NASA STI Database, the largest collection of aeronautical and space science STI in the world. The Program Office is also NASA's institutional mechanism for disseminating the results of its research and development activities. These results are published by NASA in the NASA STI Report Series, which includes the following report types:

- TECHNICAL PUBLICATION. Reports of completed research or a major significant phase of research that present the results of NASA programs and include extensive data or theoretical analysis. Includes compilations of significant scientific and technical data and information deemed to be of continuing reference value. NASA counterpart of peer-reviewed formal professional papers, but having less stringent limitations on manuscript length and extent of graphic presentations.

- TECHNICAL MEMORANDUM. Scientific and technical findings that are preliminary or of specialized interest, e.g., quick release reports, working papers, and bibliographies that contain minimal annotation. Does not contain extensive analysis.

- CONTRACTOR REPORT. Scientific and technical findings by NASA-sponsored contractors and grantees.

- CONFERENCE PUBLICATION. Collected papers from scientific and technical conferences, symposia, seminars, or other meetings sponsored or co-sponsored by NASA.

- SPECIAL PUBLICATION. Scientific, technical, or historical information from NASA programs, projects, and missions, often concerned with subjects having substantial public interest.

- TECHNICAL TRANSLATION. English-language translations of foreign scientific and technical material pertinent to NASA's mission.

Specialized services that complement the STI Program Office's diverse offerings include creating custom thesauri, building customized databases, organizing and publishing research results ... even providing videos.

For more information about the NASA STI Program Office, see the following:

- Access the NASA STI Program Home Page at ***http://www.sti.nasa.gov***

- E-mail your question via the Internet to help@sti.nasa.gov

- Fax your question to the NASA STI Help Desk at (301) 621-0134

- Phone the NASA STI Help Desk at (301) 621-0390

- Write to:
  NASA STI Help Desk
  NASA Center for AeroSpace Information
  7121 Standard Drive
  Hanover, MD 21076-1320

NASA/CR-2003-212689

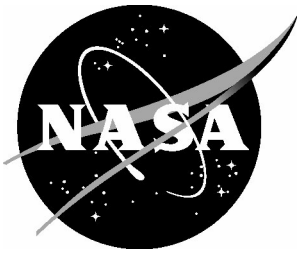

Numerical Analysis of the SCHOLAR Supersonic Combustor

Carlos G. Rodriguez
Allied Aerospace, GASL Division, Hampton, Virginia

Andrew D. Cutler
The George Washington University
Joint Institute for Advancement of Flight Sciences
Langley Research Center, Hampton, Virginia

National Aeronautics and
Space Administration

Langley Research Center
Hampton, Virginia 23681-2199

Prepared for Langley Research Center
under Contract NAS1-97110

December 2003

Available from:

NASA Center for AeroSpace Information (CASI)
7121 Standard Drive
Hanover, MD 21076-1320
(301) 621-0390

National Technical Information Service (NTIS)
5285 Port Royal Road
Springfield, VA 22161-2171
(703) 605-6000

List of Symbols

k	specific turbulence kinetic energy [m^2/s^2]
M	Mach number
p	pressure [Pa]
Pr	Prandtl number
Sc	Schmidt number
T	temperature [K]
x	axial coordinate [m]
y	vertical coordinate [m]
y_i	mass-fraction of specie i
z	lateral coordinate [m]
y^+	dimensionless vertical wall-turbulence coordinate
ρ	mass density [kg/m^3]
γ	specific-heat ratio
ω	specific dissipation rate [1/s]
τ	relative turbulence intensity
μ	viscosity [N s/m^2]

Subscripts:

L	laminar
T	turbulent
01	total inflow conditions
02	pitot value

1. Introduction

Most Computational Fluid Dynamic (CFD) codes used in practical applications are based on the Reynolds-Averaged Navier-Stokes (RANS) set of equations. These equations employ many ad hoc assumptions and empirical coefficients in the modeling of the turbulent viscous-fluxes and the chemical specie-production source-terms. Therefore, these models have to be validated with experimental data before being applied with any confidence to a given class of flows. The types of flow of interest for the present work are those found in scramjet applications.

A supersonic-combustion scramjet model known as SCHOLAR has been tested at NASA Langley's Direct-Connect Supersonic Combustion Test Facility (DCSCTF)[1,2]. This experiment was designed to provide a test case for validation of CFD codes, involving supersonic injection, mixing and combustion in a duct. The model has a simple geometry, and large regions of subsonic/recirculating are avoided; the enthalpy of the test gas corresponds to a Mach-7 flight condition (approximately 1200 K at combustor entrance). During the design of the experiment it was believed that the resulting flow would be mixing-limited (i.e., with chemical reaction towards equilibrium being much faster than the mixing process); as will be seen later, this turned out not to be the case. Some numerical simulations of this experiment have already been reported by other authors[3].

The present work documents some preliminary results in the numerical simulation of the SCHOLAR scramjet using VULCAN, a RANS computer code developed at NASA Langley[4]. The purpose of the simulation is to assess the effects of the modeling assumptions and parameters in the flowfield predictions. A brief description of the experiment and summary of the data is presented first. It is followed by the numerical analysis of the facility nozzle, which will provide the necessary inflow conditions for the simulation of the direct-connect combustor. The analysis of the scramjet proper begins with the definition of a baseline configuration for the numerical modeling. This configuration provides a reference solution which is used for a qualitative analysis of the flowfield, grid convergence study, and comparison with the data. The main objective of the investigation is to quantify the effects on this solution due to changes in some of the numerical parameters. This report concentrates on turbulence parameters such as numerical models, Schmidt and Prandtl numbers, and inflow turbulence. Future work will include the effects of chemistry models, inflow conditions and the presence of radicals.

2. Experiment

The SCHOLAR experiment has been extensively described in references 1 and 2. Only a brief description of the experimental set-up and a summary of the data will be presented here.

2.1 Description of the Facility

In the DCSCTF facility, vitiated air is produced at high enthalpy in the heater by combustion of hydrogen with premixed oxygen and air; the nominal enthalpy corresponds to Mach 7 flight. This air is accelerated through a water-cooled Mach-2 nozzle before entering the test section (operating conditions will be given later in the report). The complete layout and dimensions of the combustor model are shown in figure 1 (a). The duct consist of a constant-area isolator, which ends in a small step on the top wall. Downstream of the step there is another short constant-area section. This section is followed by a 3° divergence on the top wall, which extends all the way to the exit of the model. The span of the model is constant throughout its entire length. The injection nozzle provides hydrogen fuel at a 30° angle [figure 1 (b)]. This nozzle was designed to produce a Mach 2.5, one-dimensional flow at its exit (injection conditions and equivalence ratio to be given later). Also shown in the figure are 5 pilot injectors that were used in some runs to pilot the main injector; these injectors were not modeled in the present calculations.

The model was built in two sections: the upstream section (containing the isolator and injector) was made of copper, while the downstream section (containing most of the divergent section) was made of steel. The conductivity of these materials and the thickness of the walls allowed the duct to be run without cooling. There are 7 transverse slots in the model to allow for measurement of static temperatures fields by CARS beams; the locations shown in figure 1 (numbered 1, 3, 5, 6, 7) are the ones used in this study. The model itself is instrumented with both pressure taps and wall-temperature probes. Pressure taps are located at the centerline of the bottom wall, on the top wall (close to the sidewall for the copper section and centerline for the steel section), and on the sidewall (midpoints of the steel section). Thermocouples are located on the top wall, six for each section of the duct.

2.2 Summary of Data

Wall-pressure distributions for the pressure taps at the bottom centerline are shown in Figure 2. Data are shown at 10 s and 24 s; note that the heater is started at 1 s and fuel injection commences at 6.4 s. Comparison between measurements at these two times reveals only small differences. Also shown is the average over the total time run; this average will be used throughout the present work for comparison with numerical results. Pressures vary widely in the upstream region, probably due to the shock-wave system created by the injector and step; a small discontinuity in cross-section between nozzle and combustor, due to a stainless-steel flange, may also account for the pressure variations. Pressure generally falls moving downstream due to the divergence in the duct, until about 0.5 m. At that location it rises rapidly to a peak at about 0.75 m, and then falls slowly as the gas flows towards the exit. Very little combustion appears to take place upstream of 0.5 m, but by 0.75 m most of the mixed fuel seems to have burned; further mixing and combustion is expected to occur downstream.

Since the duct is uncooled, surface temperatures vary greatly during the course of the run; representative temperature histories and fits (top wall, unpiloted) are presented in figure 3. In the copper section, temperature is typically about 350 K at the beginning of the fuel injection and rises to as high as 600 K at the end. For the steel section, those numbers are typically 450 K and 950 K, respectively.

Figure 4 contains three-dimensional cutaway views of the duct showing contour-plots of the fitted CARS temperature data; the data are all fit to cosine-series bivariate functions. Flow-direction is from top-left to bottom-right; main fuel injector is on the top wall between planes 1 and 3. Planes 3 and 5 show a region of low temperature (between 250 and 550 K) at the center, which is the injected fuel-plume; there is no evidence of combustion between these two planes. At planes 6 and 7 temperatures have risen abruptly, suggesting near complete combustion. The hot regions at the top and bottom walls are probably near stoichiometric, with the cooler region at the center likely to be fuel-rich. Injected fuel has probably not penetrated to the sidewalls. There is some asymmetry in the data, probably due to inflow perturbations and the data fit.

3. Analysis of the Facility Nozzle

As mentioned, a two-dimensional, converging-diverging, water-cooled nozzle was used to accelerate the vitiated flow to the nominal test conditions at the combustor inlet. The conditions at the nozzle exit were probed with a pitot rake to map the pitot pressure (p_{02}). These measurements were reported in reference 5, together with comparisons to CFD calculations performed with the VULCAN code. The facility nozzle was modeled in the present work to provide inflow conditions to the duct calculations.

3.1 Solution Procedure

The three-dimensional grid used for the nozzle simulation is shown in figure 5; its dimensions are $129 \times 129 \times 145$ (axial $\times$ vertical $\times$ lateral). The half-width and full height of the nozzle was modeled, the latter because of slight asymmetries between top and bottom (curved) walls. The grid was subdivided into 32 blocks, to take advantage of the Message Passing Interface (MPI) capabilities of VULCAN. It had a wall-spacing of 5×10^{-5} m, resulting in a maximum y^+ of 65.

The inlet boundary was modeled as subsonic inflow, with a total pressure and temperature of 767250 Pa and 1828 K, respectively. The inflow turbulence intensity τ and turbulent-to-laminar viscosity ratio μ_T/μ_L were set at 25% and 600, respectively (which result in a turbulence length-scale of about 1 mm at inflow conditions). All solid (water-cooled) walls were modeled as no-slip isothermal boundaries; following reference 5, the wall-temperature was assumed to be 500 K. The exit boundary was set as supersonic extrapolation. Finally, the vertical centerplane was modeled as a symmetry boundary. As mentioned, the inflow to the nozzle was vitiated air. One-dimensional calculations assuming equilibrium and frozen compositions differed little in major species, temperature and pressure[1]. Because of this and the range of temperatures under consideration, the gas was modeled as calorically perfect in order to reduce computational expense. Following the one-dimensional results, the molecular weight and specific-heat ratio γ were assumed to be 25.9098 and 1.28909, respectively.

The inviscid fluxes were calculated using Edwards' low-dissipation flux-split scheme[6], with third-order MUSCL interpolation. Time-integration was done using the implicit diagonalized approximate-factorization scheme[7]; the entire domain was run fully elliptic. Wilcox's 1998 k-ω model and wall-matching functions[8] were used for modeling turbulent viscous stresses and heat-transfer; the turbulent Prandtl number (Pr_T) was assumed to be 0.90. Calculations were done on an SGI Origin 2000, using 32 processors. Grid sequencing with three levels was used for convergence acceleration, and also as a measure of grid convergence, as will be seen in the results. Convergence was considered to have been achieved when the residual dropped four orders of magnitude, which occurred after 1500 iterations in the fine sequence.

3.2. Results

Figure 6 shows the nozzle centerplane Mach contours. The effects of the wall asymmetry are just apparent in the contours. The calculated nozzle-exit pitot-profiles are presented in figure 7 for the vertical centerplane, and in figure 8 for the horizontal centerplane. Both show adequate agreement with the experimental data, although the latter one shows more asymmetry and thicker boundary-layers (especially in the horizontal centerplane). It should be noted the data was obtained at slightly different operating conditions than those of the SCHOLAR test used here. Also, the pitot rake was located approximately 2 mm downstream of the nozzle exit (with the duct removed); the numerical results were taken at the exit itself. Finally, measurements may be affected by the probe diameter not being small enough with respect to the boundary-layer thickness.

A detail of figure 7 is shown in figure 9 for the medium- and fine-sequence calculations, together with 1% error bars on the data. The fine-sequence solution falls within the error bars for most of the points, although the data shows a greater dip near the center. There are some differences between medium and fine calculations, but for the most part these differences are of the order of the experimental error; therefore, the solution can be considered to be grid-converged.

The values of the inflow turbulence-parameters quoted before were chosen in order to provide scramjet-inlet turbulence-intensity and viscosity-ratio of the order of 1% and 100, respectively (giving a turbulence length-scale of the order of 1 mm at exit conditions). There is no way to quantify the turbulence velocity and length scales of the experiment. To determine the effects of these parameters on the scramjet simulation, several combinations were chosen. It was found difficult to predict a priori which inflow values would give desired values at the exit, but after some trial-and-error the inflow parameters shown in table 1 were found to give adequate values at the exit potential flow (also given in the table). In particular, the values of the inflow turbulence parameters given earlier provide exit conditions with 2.5% turbulence intensity and 300 viscosity-ratio. The effects on the nozzle-exit vertical-profiles of the different combinations of turbulent parameters given in the table can be seen in figure 10. In general, higher values of τ and μ_T/μ_L appear to give better agreement with the nozzle experimental data. The effects of these parameters on the flow within the combustor proper will be shown in the next section.

4. Scramjet Baseline Solution

4.1 Solution Procedure

A reference solution was sought that would provide a first approximation to the problem, and from which parametric studies could be done. This solution, and the procedure and conditions used to obtain it, will hereafter be referred to as "baseline". Unless otherwise noted, this numerical configuration have been used for all calculations reported here.

The half-width combustor was discretized with a grid that had approximately 3.6 million control volumes (CVs), uniformly distributed among 80 blocks (again, to take advantage VULCAN's MPI capability). A detail of the grid in the neighborhood of the injector is shown in figure 11. To reduce grid requirements, non-C(0) block-boundaries were extensively used (as may be seen from the grid discontinuities in the figure). The vertical grid-dimensions varied between 61 and 85, and the lateral between 61 and 81. The grid spacing at the wall varied between 1.5×10^{-4} m and 3.0×10^{-4} m. For the most part, the resulting values of y^+ are below 100, which is just about right for the use of wall functions.

For inflow conditions at the combustor inlet, the profiles obtained from the nozzle calculation were imposed on the boundary. To allow for multi-species calculations, species mass-fractions were added. The vitiated composition from the one-dimensional calculations previously mentioned included about two dozen species. For the chemistry models used in the present calculations (which could not account for most of the vitiation species), the inflow was assumed to contain only N_2, O_2 and H_2O with uniform mass-fractions 0.5638, 0.2321 and 0.2041, respectively[a]; these were obtained from the one-dimensional analysis using the same mole fractions for O_2 and H_2O (the mole fraction of N_2 was slightly adjusted to give a total mole-fraction of 1.0). The inflow conditions at the inlet of the hydrogen injector were assumed to be subsonic with total pressure and temperature of 3.44 MPa and 302 K, respectively. These conditions resulted in an equivalence ratio of approximately 1.0. The solid walls were modeled as no-slip isothermal, with wall temperatures set at 400 K and 500 K for the copper and steel sections, respectively (based on the wall-temperatures shown in figure 3). The exit boundary was modeled as supersonic extrapolation, and the vertical centerplane was modeled as a symmetry boundary.

The inviscid space and time integration schemes were the same as for the nozzle calculations, unless otherwise noted. The burner was ran fully-elliptic, to account for possible subsonic/recirculation regions; some calculations were done using a semi-elliptic approach to be described below. The flow was modeled as a mixture of thermally-perfect gases. The chemistry model used was Drummond's 9-specie/18-reaction (9×18) mechanism[9]; the ignition-region feature in VULCAN was needed to ignite this model at the present conditions. Thermodynamic properties of the chemical species were modeled with a one-curve polynomial fit included in VULCAN, and based on the data from reference 10. The Wilcox k-ω turbulence model and wall functions were again used. They were supplemented with the Wilcox compressibility correction, used to reduce spreading rates (or turbulence) as a function of the local turbulence Mach number[8]. Not included was the Pope correction for the round-jet/plane-jet anomaly, which is standard in Wilcox's model. The turbulence Prandtl (Pr_T) and Schmidt (Sc_T) numbers were set at 1.0.

A three-level grid sequencing was again used for convergence acceleration and to estimate grid convergence. Computations were done on 80 500-MHz processors of an SGI Origin 2000 computer; the

[a]The effects of radicals such as OH present in the inflow will be the subject of future work.

ideal parallel speed-up obtained with the present grid was 78.3. Also used were 16 DEC Alpha 667 MHz nodes in a BEOWULF cluster.

4.2. Results

A total of 10,000 iterations were done on the medium sequence, and 45,000 on the fine sequence. For both sequences, the residual would drop about two orders of magnitude before undergoing slow oscillations. For the medium-grid solution, convergence was assumed when no variation would be observed in either the overall flowfield or the wall-pressure distributions; the solution was mostly converged after 2,000-3,000 iterations. For the fine-grid solution, a minimum of 35,000 were needed before the solution would show no further changes.

Figure 12 shows the centerplane Mach contours for the baseline solution (note that in this and subsequent centerplane plots the vertical scale is twice the horizontal for better resolution). The jet penetrates at approximately 30° for a certain distance, but it is immediately turned in the direction of the main flow while continuing to penetrate further towards the opposite wall. The expansion after the step, and compression from the jet are clearly seen. A region of slower flow is apparent downstream of x ~ 0.50 m.

The water mass-fraction contours (figure 13) suggests that ignition takes place between 0.45 and 0.5 m. This is also shown by the temperature contour plots (figure 14). The CARS measurements samples only indicate that heat-release occurs after 0.4 m. The fuel core (indicated by the low-temperature regions) seems to penetrate further in the numerical simulation. The mixing and combustion efficiency distributions are presented in figure 15; they are defined[11] as mixed-fuel over total-fuel, and reacted (water)-fuel over total-fuel, respectively, and corrected for vitiation[12]. Initially, the combustion lags with respect to the mixing, but it raises rapidly after 0.5 m, and by 0.8 m most of the mixed fuel appears to have reacted. Overall, just over 60% of the fuel seems to mix and react with the inflow air.

These observations are confirmed by the analysis of the bottom-wall centerline pressure distribution (figure 16). The experimental data sampling can only locate the ignition delay somewhere between 0.45 and 0.57 m. CFD predicts the flame to begin near the upstream limit; this is likely to be an underprediction of the delay. The pressure levels from the medium- and fine-sequence solutions are compared in figure 17. At the inlet, the medium-solution levels are slightly higher than the fine-solution; this has been observed in other VULCAN calculations[13], and may be due to post-processing of the medium-sequence solution. The main difference between both solutions is in the ignition delay, which is considerably greater for the medium solution (and closer to the data). This is counter-intuitive, since the greater numerical diffusion of the coarser grid should result in greater mixing, and therefore less ignition delay (see below). In any case, these results show that grid convergence at the very least has not been proven on the current grid.

This preliminary solution indicates that the baseline model likely underpredicts the ignition delay, or time for a fuel-air mixture to form a flame in the absence of ignition sources[14]. This delay is the combination of a physical delay (depending on fuel mixing) and a chemical delay (time for flame production after the formation of a homogeneous fuel-air mixture). In the numerical solution, the former mostly depends on the turbulence model and the latter on the chemistry model. Therefore, the underprediction of the ignition delay may be due to an overprediction of the mixing by the turbulence model, an underprediction of the chemical delay by the chemistry model, or a combination of both. Another deficiency is the overprediction of the penetration of the fuel plume; it is likely due to the turbulence model, although this is subject to further verification.

Some of the following calculations were obtained with a "semi-elliptic" integration approach, in order to reduce computational requirements. In this approach, the first 48 upstream blocks were solved elliptically, with a first-order extrapolation boundary-condition applied at the downstream end of the resulting region (at x ~ 0.35 m). Convergence on this region was fairly rapid, owing to the absence of significant reaction. The remaining 32 blocks were then solved, also elliptically, for about 15,000-20,000 iterations. The results for the baseline condition are shown in figures 18 and 19. The solution is almost indistinguishable from the fully-elliptic calculation. Since most of the computation is spent in the second (reacting) region, this approach reduces the computational effort by almost 60%. The calculations performed with this approach will be explicitly noted.

As explained in the Introduction, for the present work the effects in the turbulence parameters were studied. Two additional turbulence models were tested: Menter's k-ω model[15], and an explicit algebraic stress model extension[b] (EASM) of the Wilcox model based on Gatski and Speziale's model[16]; these calculations were done using the semi-elliptic integration described above. Menter's model combines the Wilcox k-ω model near solid walls, with the standard k-ε model everywhere else (particularly in shear-dominated flow-regions). The results for this model (figures 20 and 21) show that it slightly overpredicts ignition delay, and has less fuel-plume penetration than the Wilcox model. On the other hand, it considerably overpredicts the pressure-rise in the reaction region. The EASM model is essentially an extension of the Boussinesq approximation, providing a non-linear constitutive relation between turbulent stresses and strain-rates. They account for the anisotropy of the normal Reynolds stresses, which in turn allows for the simulation of stress-induced motions. These motions are of importance in corner-flow regions, were they may delay the onset of separation due to adverse pressure gradients. For the present application, it can be seen (figures 22 and 23) that the EASM model provides an acceptable approximation to the ignition delay and pressure-rise, but at the expense of overpredicting the fuel-plume penetration.

The effects of lowering Sc_T and Pr_T by half from their baseline values are shown in figures 24 to 27. Lowering Sc_T (figures 24 and 25) appears to have little impact on fuel-plume penetration, but the ignition-delay and pressure-rise predictions are unacceptable. On the other hand, a lower Pr_T has little effect on pressure-rise and ignition-delay while having a somewhat lower penetration of the fuel-plume. The values $Pr_T = Sc_T = 0.50$ are usually recommended for shear-dominated flows[17]. No attempt was made to test values higher than the baseline ones, since it was considered that these were already high enough.

The effects of the different combinations of inflow turbulence-parameters of table 1 are given in figures 28 to 31. The high-turbulence inflow (figures 28 and 29), which appeared to give better agreement with the nozzle data, is shown here to give a somewhat better approximation to jet-penetration, at the expense of the agreement with ignition delay and pressure-rise. The low-turbulence inflow (figures 30 and 31) seems to overpredict ignition delay and penetration, and somewhat underpredict pressure-rise. In brief, a change of approximately 50% in τ and a factor of 3 in μ_T/μ_L with respect to baseline values can give drastically different solutions. These parameters are not usually estimated in experiments, and in any case can only be done so in an order-of-magnitude basis.

One common thread through all these calculations is the apparent inability of current turbulence-modeling to accurately predict ignition delay, combustion pressure-rise and fuel-plume penetration simultaneously. So far, only two of the three parameters at best could be adequately captured.

[b]It should be noted that this model is still under development within VULCAN.

5. Conclusions

The SCHOLAR scramjet is the subject of an ongoing numerical investigation, with the purpose of validating the VULCAN code and its turbulence and chemistry models. The facility nozzle was modeled first, in order to provide adequate inflow conditions to the combustor. Results for the latter show that CFD could predict its qualitative behavior, particularly reaction-limited heat-release due to ignition delay. From a quantitative point of view, at least two problems were identified: the inability to prove grid-convergence for the grid currently used, and the difficulty of accurately predicting all three parameters relevant for the present application: ignition delay, combustion pressure-rise, and fuel-plume penetration.

Regarding grid convergence, this could not be proved using simple grid-sequencing. Additionally, the trends between the sequences were not what would be expected in terms of numerical diffusion. One possible cause for this behavior could be in the extensive use of non-C(0) zonal boundaries, both normal and parallel to the flow. The latter ones could adversely affect the numerical flowfield by introducing extended areas of numerical diffusion.

The second problem is associated with the accuracy of turbulence and chemistry models. Only the first ones were investigated here, and the numerical solution was shown to be sensitive to them. Different turbulence models gave qualitatively dissimilar solutions. Furthermore, a relatively high value of 1.0 had to be used for the turbulent Schmidt number, if the ignition delay was to be captured at all. Another issue is that of inflow turbulence-parameters. These are not usually determined in experiments, and appear to have a considerable impact in numerical solutions. It is not immediately obvious what combination, if any, of modeling parameters would allow to simultaneously predict the three flow-parameters mentioned above with any acceptable accuracy.

Future work will initially concentrate on obtaining a grid-converged solution. A new grid is under development in which the discontinuous boundaries have been restricted to a limited number normal to the flow; the computational price to pay is an almost doubling of the total number of CVs. Based on the results from this grid, it will be determined whether the numerical results obtained so far are valid or need to be recalculated. The next step will be to include the effects of chemistry parameters as described in the Introduction. The overall objective will be to determine the sensibility of the solution to the different parameters present in most numerical models, and perhaps establish an “envelope” in some solution space were the “correct” answer may be expected.

References

1. Cutler, A.D., Danehy, P.M., Springer, R.R., DeLoach, R., and Capriotti, D.P., “CARS Thermometry in a Supersonic Combustor for CFD Code Validation”, AIAA Paper 2002-0743, 2002.

2. Cutler, A.D., Diskin, G.S., Danehy, P.M., and Drummond, J.P., “Fundamental Mixing and Combustion Experiments for Propelled Hypersonic Flight”, AIAA Paper 2002-3879, 2002.

3. Drummond, J.P., Diskin, G.S., and Cutler, A.D., “Fuel-Air Mixing and Combustion in Scramjets”, AIAA Paper 2002-3878, 2002.

4. White, J.A., and Morrison, J.H., “A Pseudo-Temporal Multi-Grid Relaxation Scheme for Solving the Parabolized navier-Stokes Equations”, AIAA 99-3360, 1999.

5. Springer, R.R., Cutler, A.D., Diskin, G.S., and Smith, M.W., “Conventional/Laser Diagnostics to Assess Flow Quality in A Combustion-Heated Facility”, AIAA Paper 99-2170.

6. Edwards, J.R., “A Low-Diffusion Flux-Splitting Scheme for Navier-Stokes Calculations”, *Computers and Fluids*, Vol. 26, No. 6, 1997, pp. 635-659.

7. Pulliam, T.H., and Chaussee, D.S., “A Diagonal Form of an Implicit Approximate-Factorization Algorithm”, *Journal of Computational Physics*, Vol. 39, Feb. 1981, pp. 347-363.

8. Wilcox, D.C., *Turbulence Modeling for CFD*, 2nd. Edition, DCW Industries, Inc., 1998.

9. Drummond, J.P., “A Two-Dimensional Numerical Simulation of a Supersonic, Chemically Reacting Mixing Layer”, NASA TM 4055, 1988.

10. McBride, B.J., Heimel, S., Ehlers, J.G., and Gordon, S., “Thermodynamic Properties to 6000 K for 210 Substances Involving the First 18 Elements”, NASA SP-3001, 1963.

11. Rogers, R.C., “A Study of the Mixing of Hydrogen Injected Normal to a Supersonic Airstream”, NASA TN D-6114, 1971.

12. Srinivasan, S., and Erickson, W., “Interpretation of Vitiation Effects on Testing at Mach 7 Flight Conditions”, AIAA 95-2719, 1995.

13. Rodriguez, C.G., “CFD Analysis of the CIAM/NASA Scramjet”, AIAA 2002-4128, 2002.

14. Laster, W.R., and Sojka, P.E., “Autoignition of H_2-Air: The Effect of NO_x Addition”, *Journal of Propulsion and Power*, Vol. 5, No. 4, July-August 1989, pp. 385-390.

15. Menter, F.R., “Improved Two-Equation k-ω Turbulence Models for Aerodynamic Flows”, NASA TM 103975, October 1992.

16. Gatski, T.B., and Speziale, C.G., “On Explicit Algebraic Stress Models for Complex Turbulent Flows”, Journal of Fluid Mechanics, Vol.254, 1993, pp. 59-78.

17. Schetz, J.A., *Boundary Layer Analysis*, Prentice-Hall, New jersey, 1993.

Tables

Table 1. Nozzle Inflow and Outflow Turbulence Parameters

Description[*]	**Inlet**		**Exit**[†]	
	τ	μ_T/μ_L	τ	μ_T/μ_L
Baseline	0.25	600	0.025	300
High turbulence	0.10	600	0.035	850
Low turbulence	0.25	300	0.015	100

[*]Based on exit conditions
[†]Values are approximate potential-core averages.

Figures

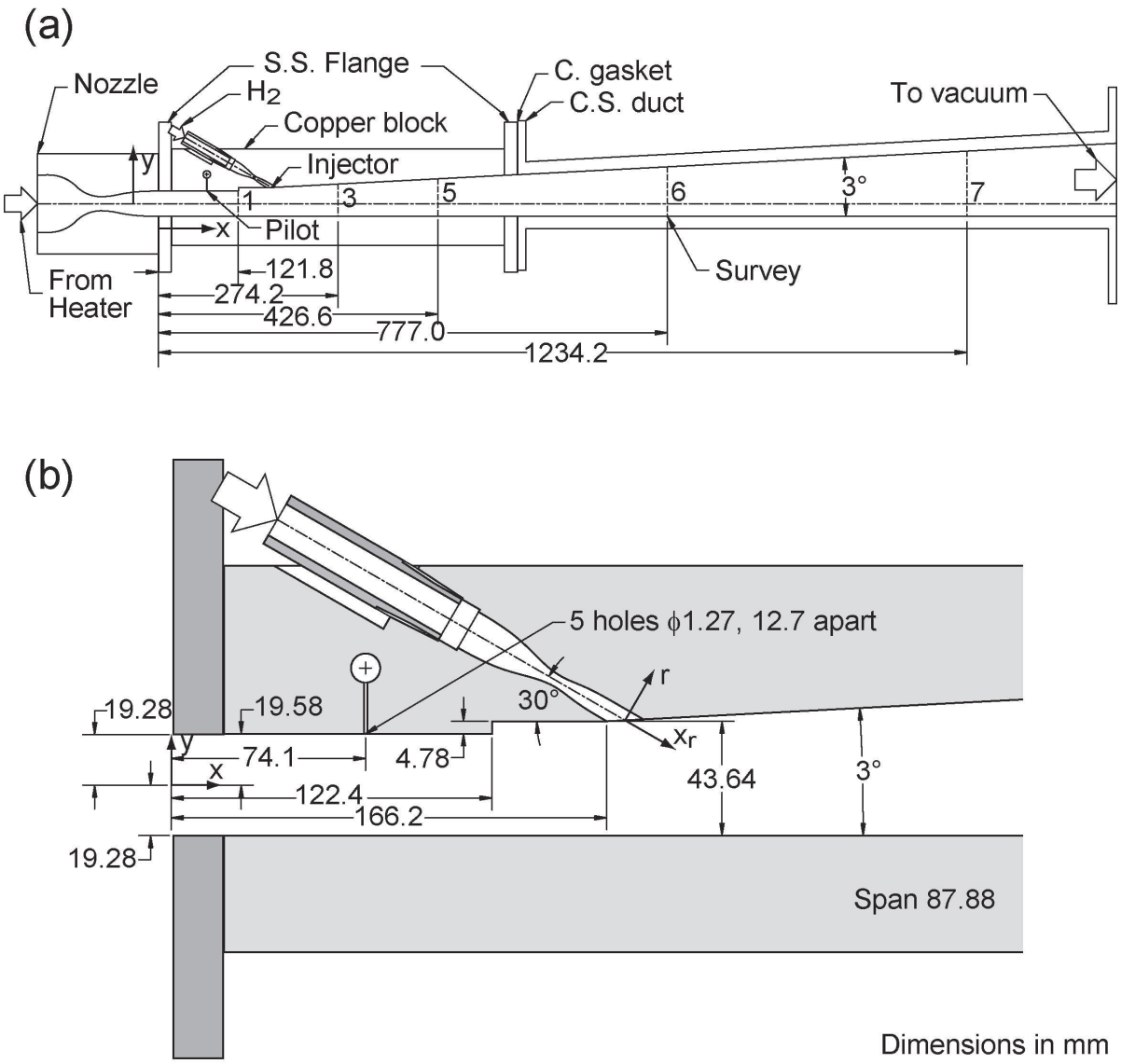

Figure 1. Layout of the combustor model:
(a) Nozzle and complete combustor. (b) Detail in the region of the injector.

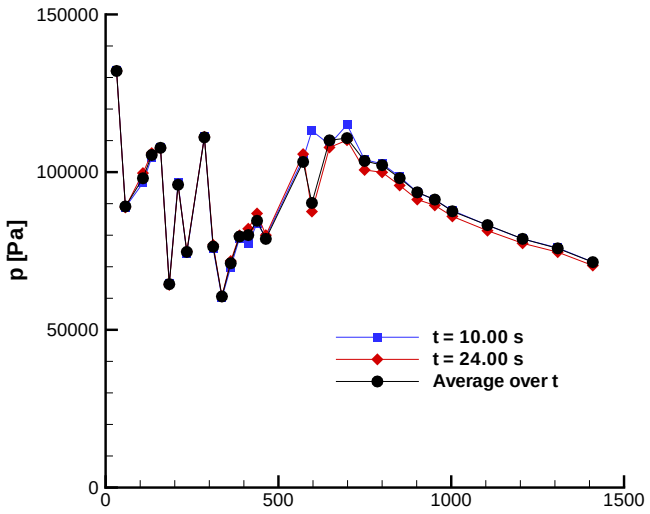

Figure 2. Bottom-wall experimental pressure distributions.

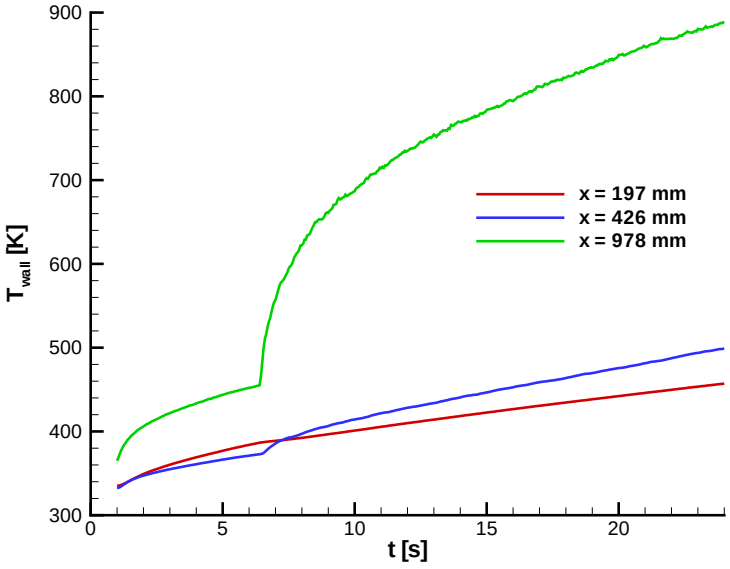

Figure 3. Top-wall temperature history.

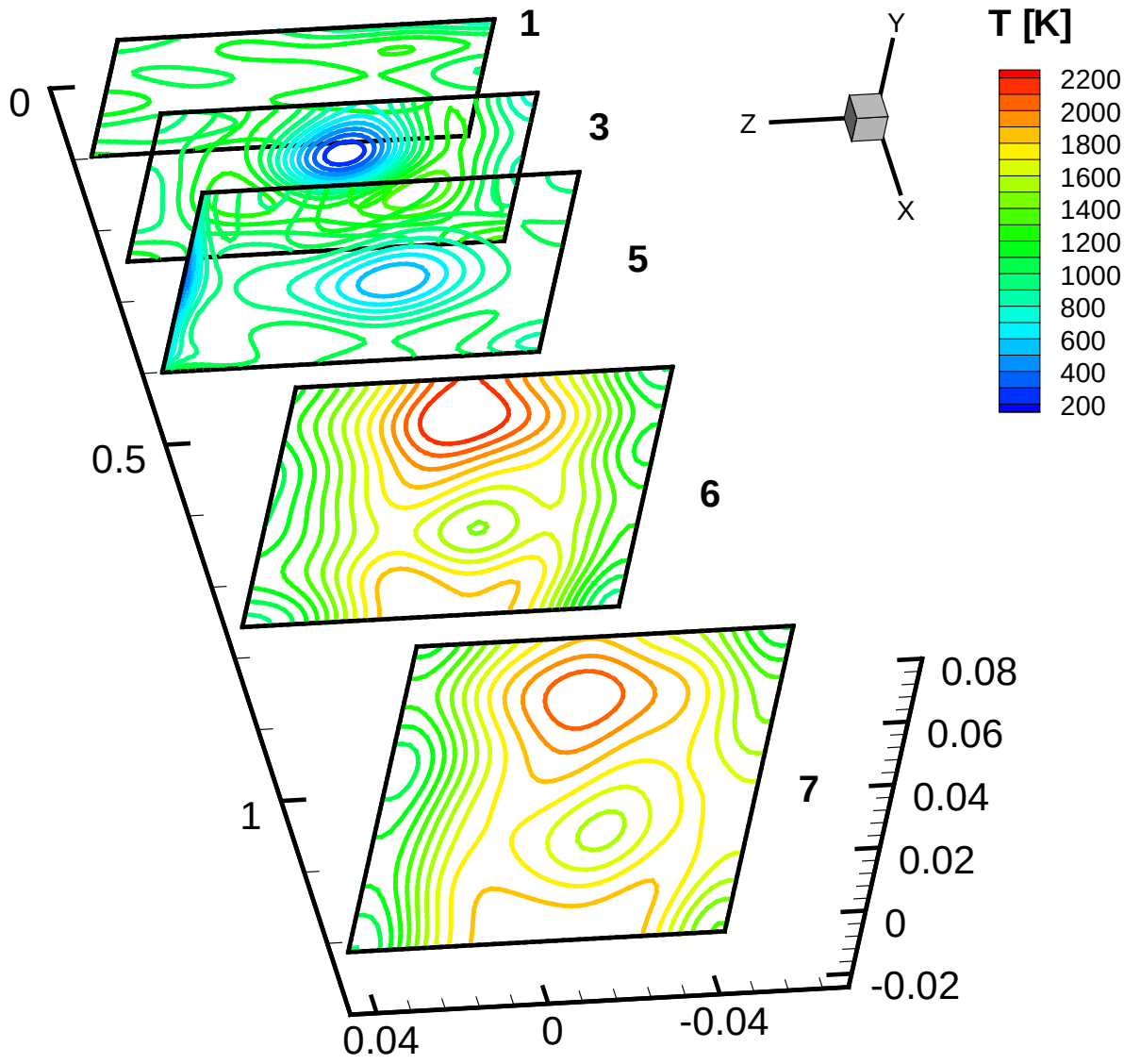

Figure 4. Cutaway planes with contours of mean temperature (dimensions in meters).

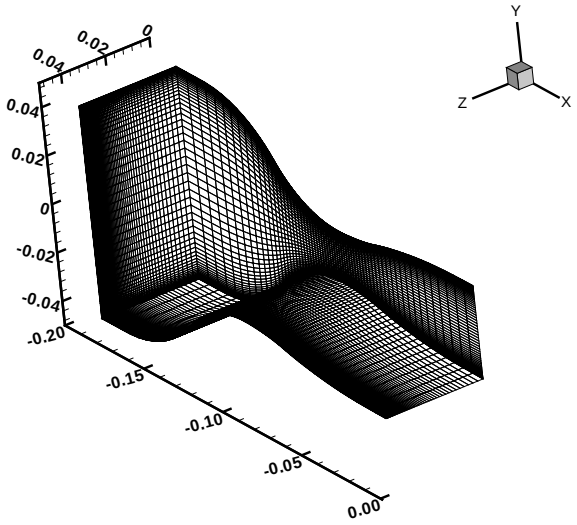

Figure 5. Three-dimensional nozzle grid (every other grid-line shown).

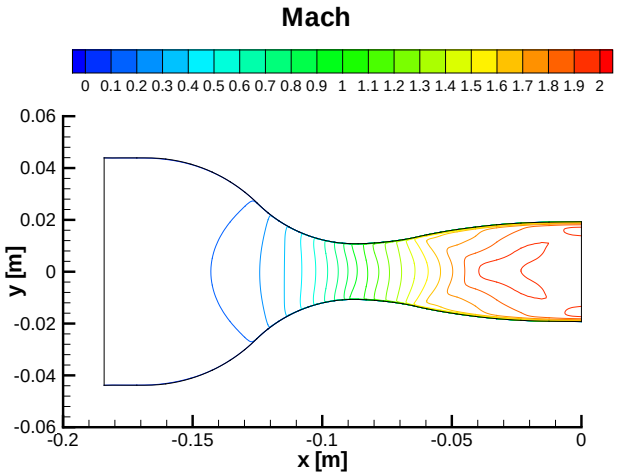

Figure 6. Nozzle centerplane Mach contours.

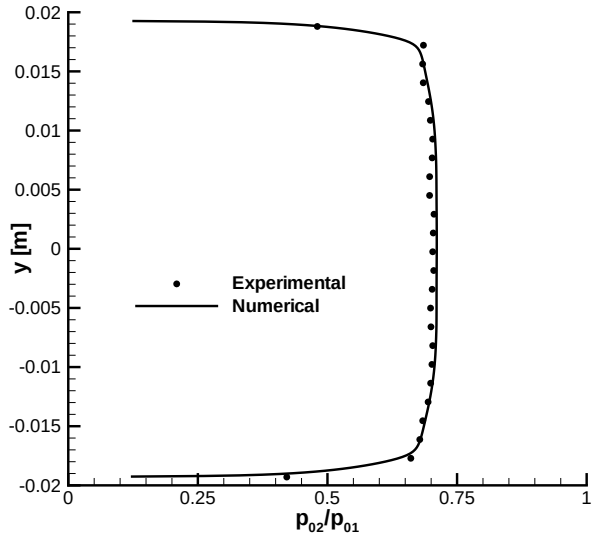

Figure 7. Nozzle vertical-centerplane pitot-pressure profiles.

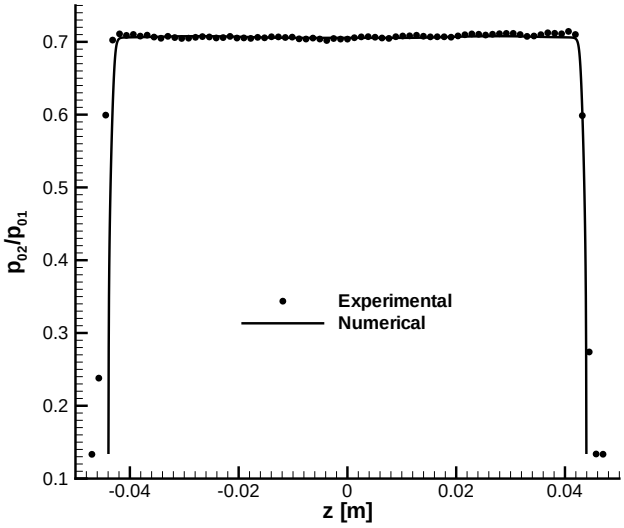

Figure 8. Nozzle horizontal-centerplane pitot-pressure profiles.

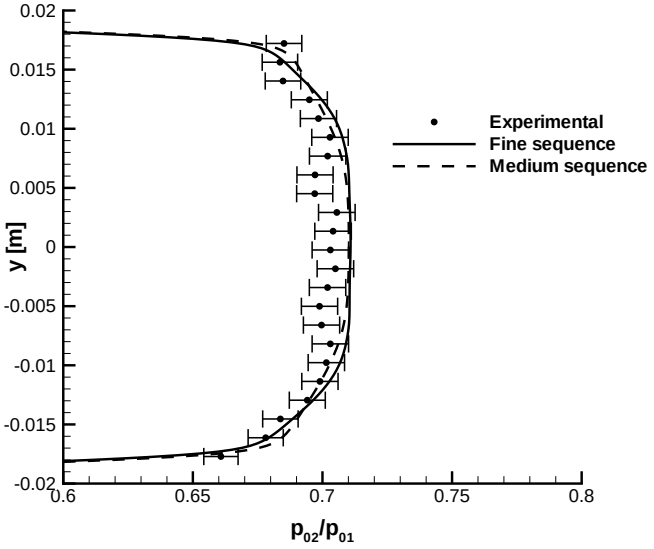

Figure 9. Nozzle vertical-centerplane pitot-pressure profiles: grid sequencing.

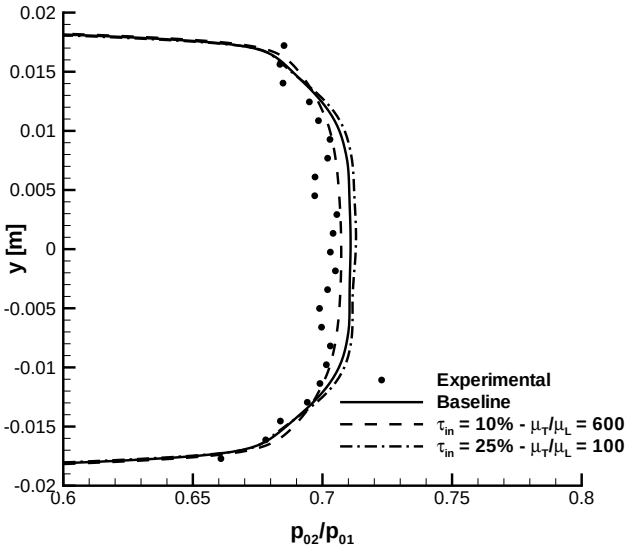

Figure 10. Nozzle vertical-centerplane pitot-pressure profiles: effects of inflow turbulence.

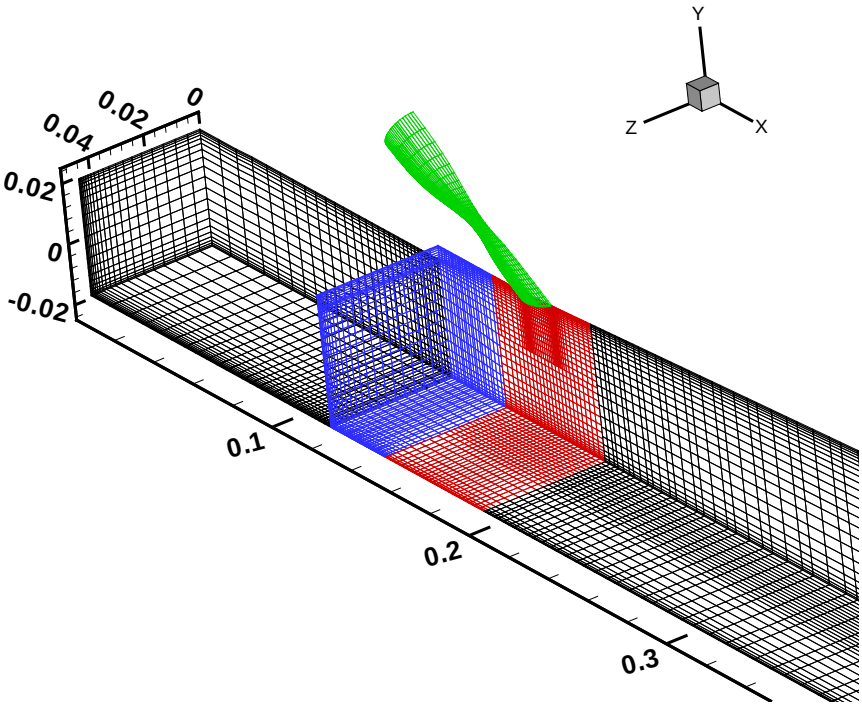

Figure 11. Scramjet: three-dimensional grid (every third grid-line shown).

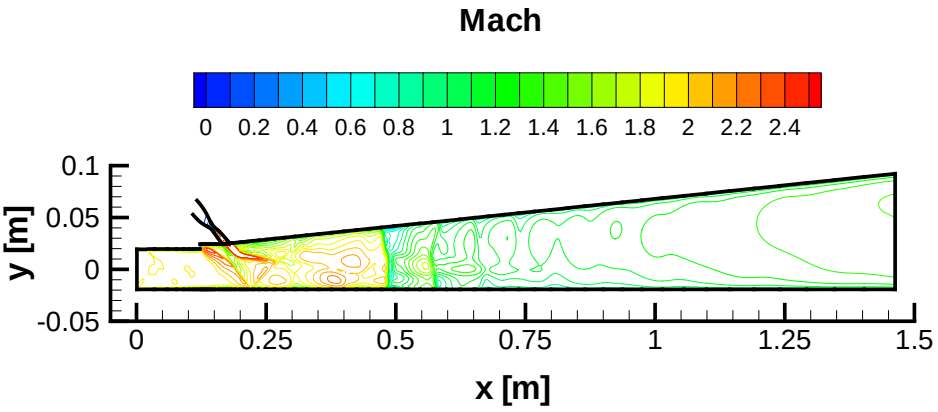

Figure 12. Centerplane Mach contours - baseline solution.

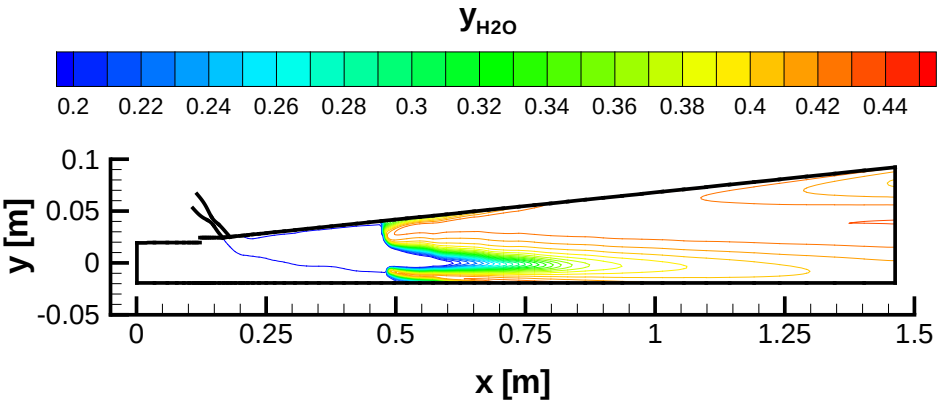

Figure 13. Centerplane water contours - baseline solution.

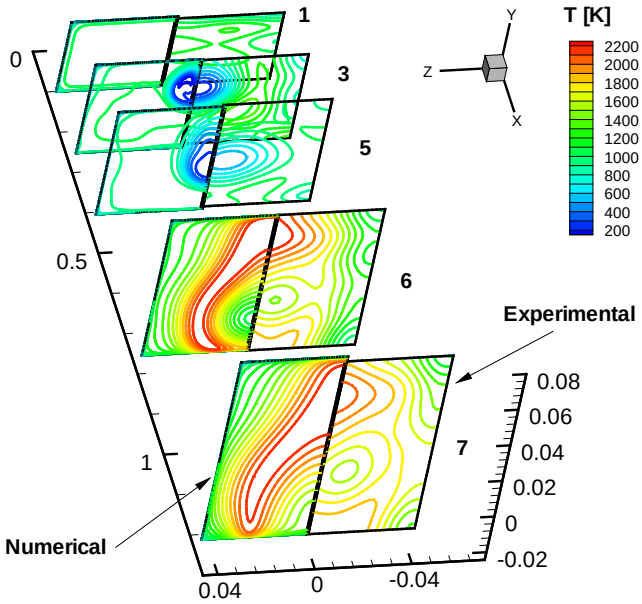

Figure 14. Temperature contours - baseline solution.

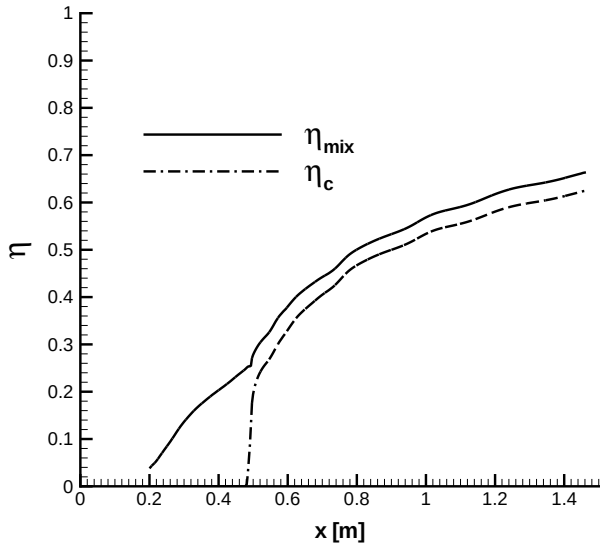

Figure 15. Efficiencies distributions - baseline solution.

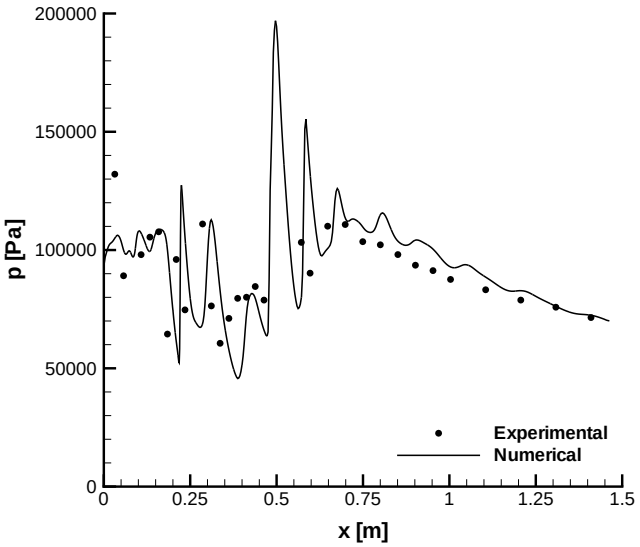

Figure 16. Bottom-wall centerline pressures- baseline solution.

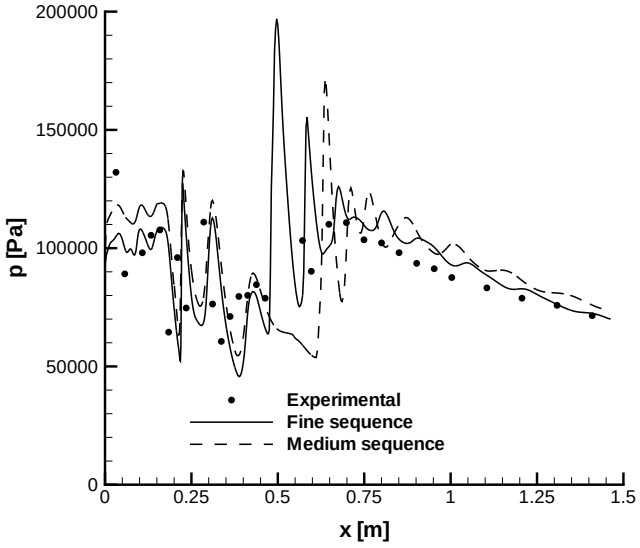

Figure 17. Effect of grid sequencing on wall-pressures - baseline solution.

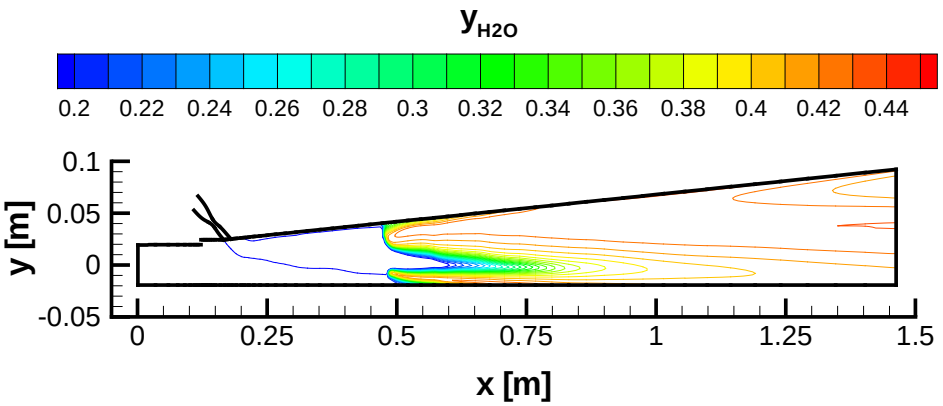

Figure 18. Water contours - Semi-elliptic integration.

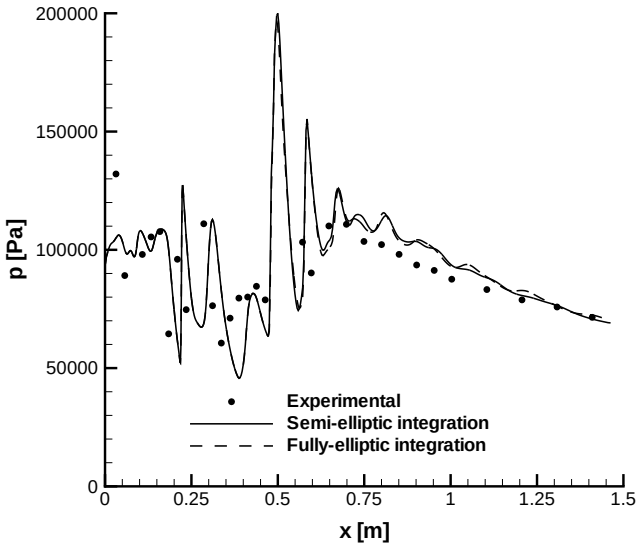

Figure 19. Wall-pressure distribution - Semi-elliptic integration.

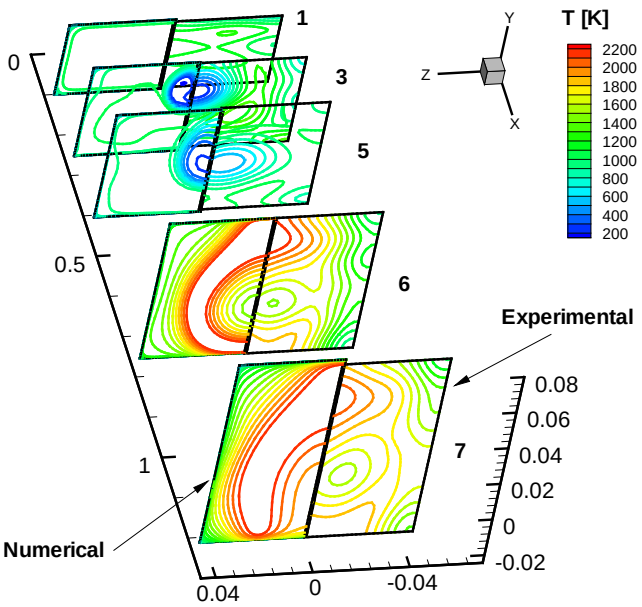

Figure 20. Temperature contours - Menter's turbulence model.

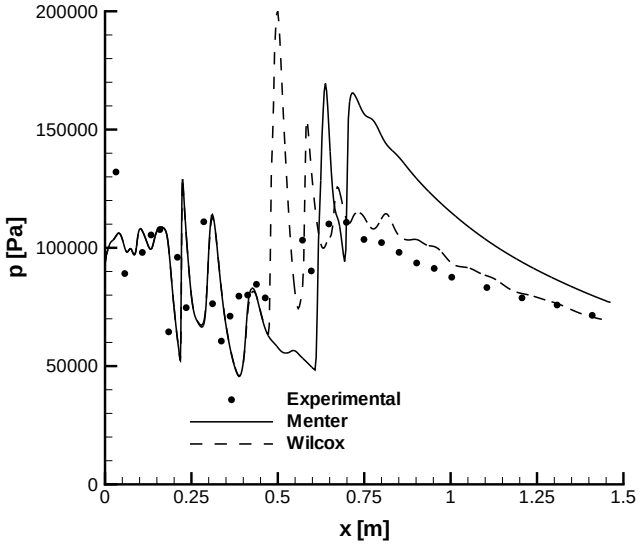

Figure 21. Wall-pressure distribution - Menter's turbulence model.

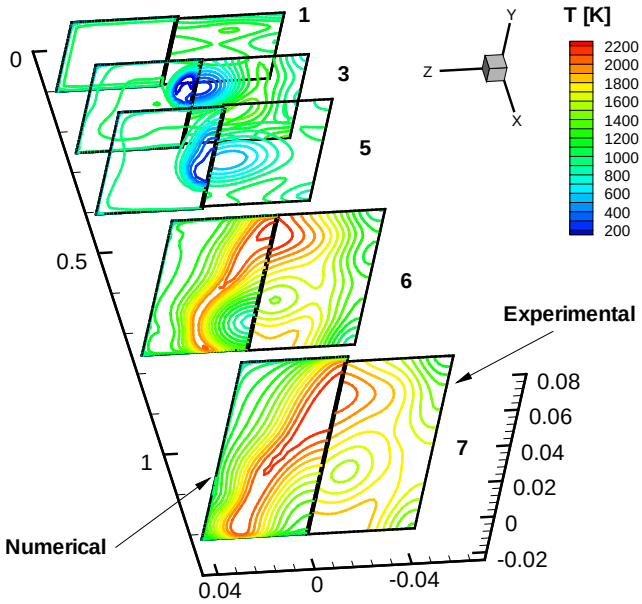

Figure 22. Temperature contours - EASM turbulence model.

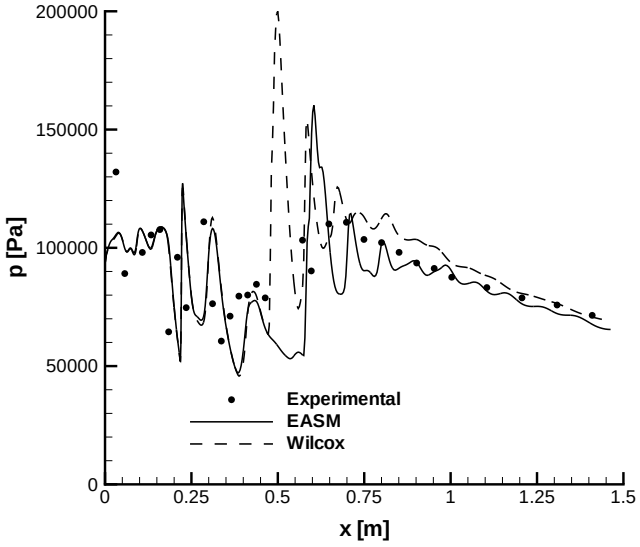

Figure 23. Wall-pressure distribution - EASM turbulence model.

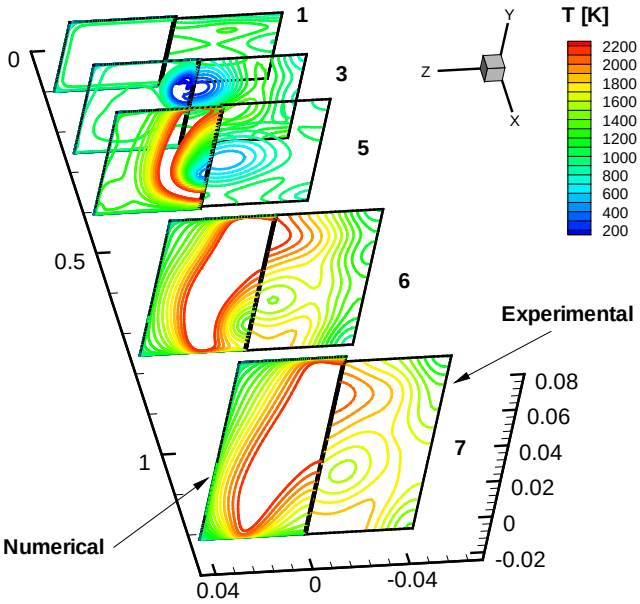

Figure 24. Temperature contours - Sc = 0.50.

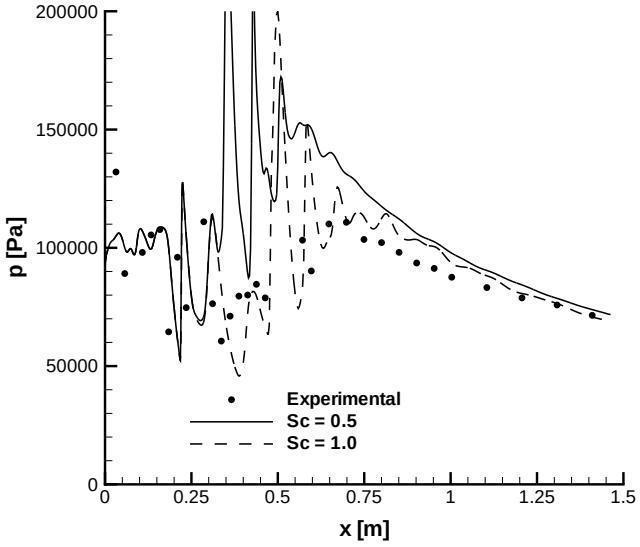

Figure 25. Wall-pressure distribution - Sc = 0.50.

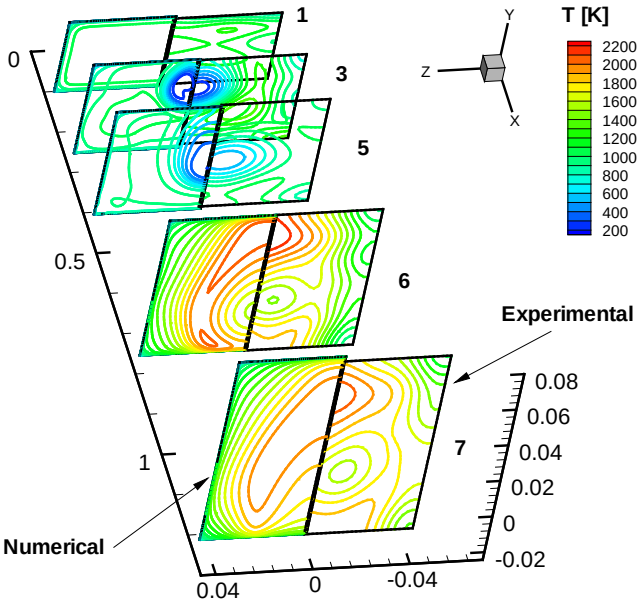

Figure 26. Temperature contours - Pr = 0.50.

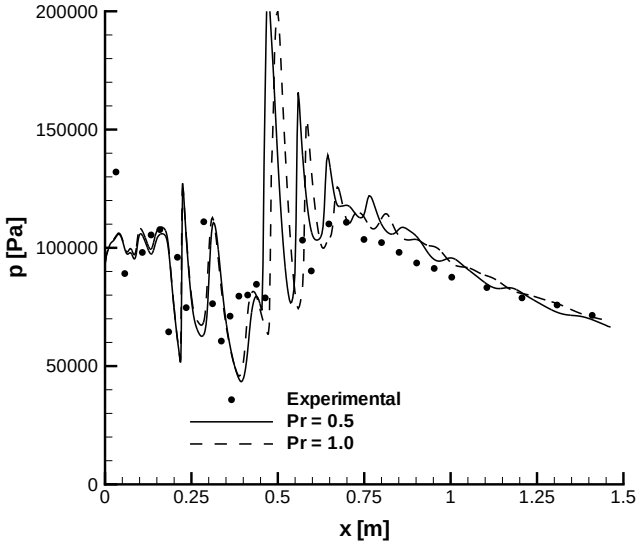

Figure 27. Wall-pressure distribution - Pr = 0.50.

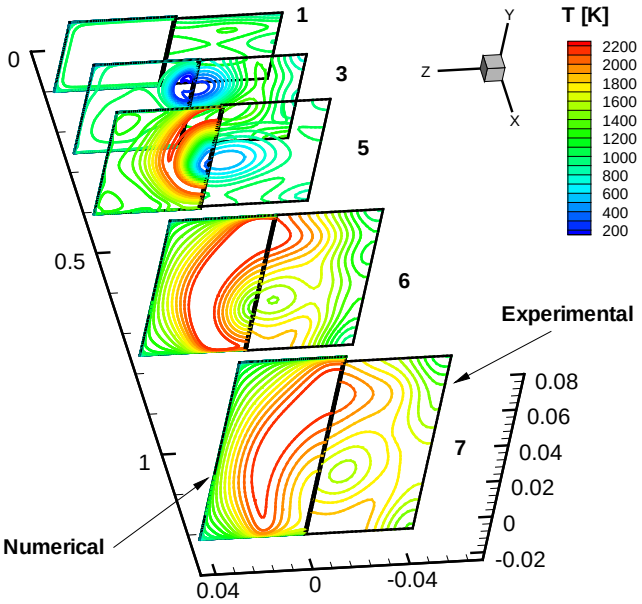

Figure 28. Temperature contours - High inflow-turbulence.

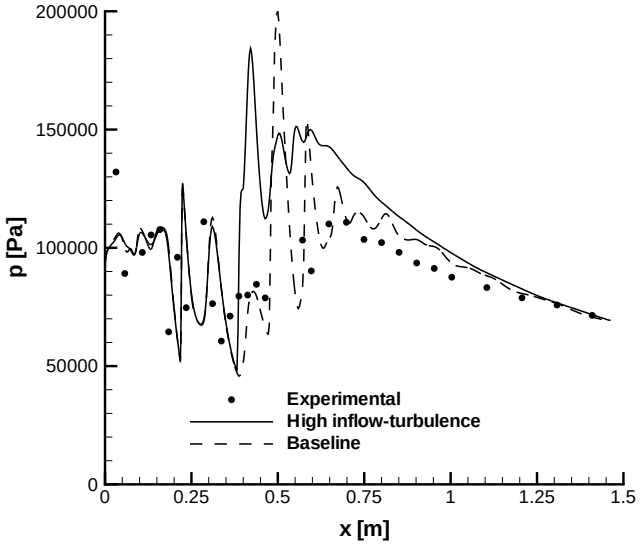

Figure 29. Wall-pressure distribution - High inflow-turbulence.

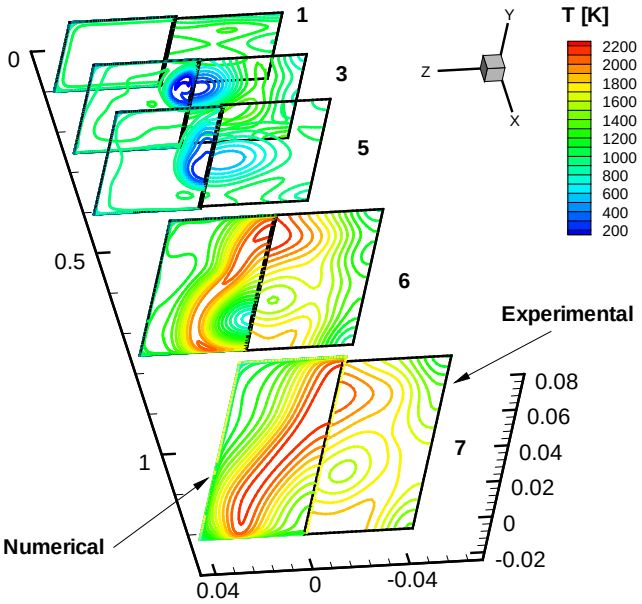

Figure 30. Temperature contours - Low inflow-turbulence.

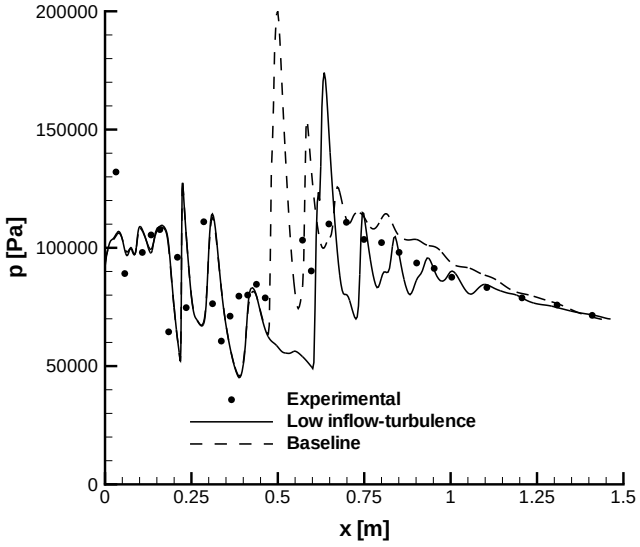

Figure 31. Wall-pressure distribution - Low inflow-turbulence.

REPORT DOCUMENTATION PAGE

Form Approved
OMB No. 0704-0188

1. REPORT DATE *(DD-MM-YYYY)*	2. REPORT TYPE	3. DATES COVERED *(From - To)*
01- 12 - 2003	Contractor Report	

4. TITLE AND SUBTITLE
Numerical Analysis of the SCHOLAR Supersonic Combustor

5a. CONTRACT NUMBER
NAS1-97110

5b. GRANT NUMBER

5c. PROGRAM ELEMENT NUMBER

6. AUTHOR(S)
Rodriguez, Carlos G.; Cutler, Andrew D.

5d. PROJECT NUMBER

5e. TASK NUMBER

5f. WORK UNIT NUMBER
23-745-30-10

7. PERFORMING ORGANIZATION NAME(S) AND ADDRESS(ES)
Allied Aerospace, GASL Division, Hampton, VA 23681-2199
The George Washington University, JIAFS, Hampton, VA 23681-2199
NASA Langley Research Center, Hampton, VA 23681-2199

8. PERFORMING ORGANIZATION REPORT NUMBER

9. SPONSORING/MONITORING AGENCY NAME(S) AND ADDRESS(ES)
National Aeronautics and Space Administration
Washington, DC 20546-0001

10. SPONSOR/MONITOR'S ACRONYM(S)
NASA

11. SPONSOR/MONITOR'S REPORT NUMBER(S)
NASA/CR-2003-212689

12. DISTRIBUTION/AVAILABILITY STATEMENT
Unclassified - Unlimited
Subject Category 34
Availability: NASA CASI (301) 621-0390 Distribution: Nonstandard

13. SUPPLEMENTARY NOTES
Rodriguez: Allied Aerospace; Cutler: The George Washington University
Langley Technical Monitor: David E. Reubush
An electronic version can be found at http://techreports.larc.nasa.gov/ltrs/ or http://ntrs.nasa.gov

14. ABSTRACT

The SCHOLAR scramjet experiment is the subject of an ongoing numerical investigation. The facility nozzle and combustor were solved separate and sequentially, with the exit conditions of the former used as inlet conditions for the latter. A baseline configuration for the numerical model was compared with the available experimental data. It was found that ignition-delay was underpredicted and fuel-plume penetration overpredicted, while the pressure rise was close to experimental values. In addition, grid-convergence by means of grid-sequencing could not be established. The effects of the different turbulence parameters were quantified. It was found that it was not possible to simultaneously predict the three main parameters of this flow: pressure-rise, ignition-delay, and fuel-plume penetration.

15. SUBJECT TERMS
Supersonic combustion; Scramjet; Computational fluid dynamics; Turbulence

16. SECURITY CLASSIFICATION OF:			17. LIMITATION OF ABSTRACT	18. NUMBER OF PAGES	19a. NAME OF RESPONSIBLE PERSON
a. REPORT	b. ABSTRACT	c. THIS PAGE			STI Help Desk (email: help@sti.nasa.gov)
					19b. TELEPHONE NUMBER *(Include area code)*
U	U	U	UU	35	(301) 621-0390